Combined Experimental and Master Equation Investigation of the Multiwell Reaction H + SO_2†

Mark A. Blitz,‡ Kevin J. Hughes,‡ Michael J. Pilling,*,‡ and Struan H. Robertson‡,§

School of Chemistry, University of Leeds, Leeds, LS2 9JT, U.K., and Accelrys Inc., 334, Cambridge Science Park, Cambridge, CB4 0WN, U.K.

Received: August 22, 2005; In Final Form: November 11, 2005

The temperature and pressure dependence of the rate coefficient for the reaction H + SO_2 has been measured using a laser flash photolysis/laser-induced fluorescence technique, for $295 \leq T/K \leq 423$ and for $3 \leq [He]/10^{18}$ molecules $cm^{-3} \leq 23$. Under these conditions, the reaction occurs exclusively to form HSO_2. These data have been fitted to, and used to refine, a master equation (ME) model of the H + SO_2 reaction system that includes the isomers HSO_2 and HOSO and the high-temperature products OH + SO. The potential energy for the system is based on literature ab initio calculations. The three eigenvalues of lowest magnitude, obtained from solution of the ME, are the chemically significant eigenvalues that are related to the pressure and temperature dependent rate coefficients for the chemical system. The eigenvalues are generally well separated from each other and from the eigenvalues relating to collisional relaxation, except at high temperatures. The rate coefficients were extracted from the eigenpairs of the ME solution, using an analysis developed by Klippenstein and Miller (*J. Phys. Chem. A* **2002**, *106*, 9267) and an adaptation of an earlier analysis by Bartis and Widom (*J. Chem. Phys.* **1974**, *60*, 3474). The relationship between the temperature dependence of the chemically significant eigenvalues and combinations of rate coefficients was elucidated via an approximate analysis of the chemical rate equations and it was demonstrated that each eigenvalue relates primarily to passage over a single transition state. Some problems were encountered in equating ratios of rate coefficients for forward and reverse reactions to the equilibrium constant. This problem arises from the nonconservative nature of the reaction system; it was resolved by imposing orthogonality on the coupled rate equations of the chemical system, giving good agreement between rate coefficient ratios and equilibrium constants. The temperature and pressure dependences of the rate coefficients were parametrized according to Troe and modified Troe expressions. The key processes, from a combustion perspective, are the formation and dissociation of HOSO and the formation of OH + SO. Except at pressures $>10^3$ atm, the latter proceeds directly from H + SO_2, via the energized states of HOSO. The derived rate coefficients rely heavily on measurements of the reverse reaction, OH + SO, which has only been determined at temperatures up to 700 K.

1. Introduction

The reaction of H atoms with SO_2 proceeds via a multistep mechanism, involving the isomer adducts HSO_2 and HOSO:

$$H + SO_2 \rightleftharpoons HSO_2 \quad \text{(R1)}$$

$$H + SO_2 \rightleftharpoons HOSO \quad \text{(R2)}$$

$$H + SO_2 \rightarrow OH + SO \quad \text{(R3)}$$

$$HSO_2 \rightleftharpoons HOSO \quad \text{(R4)}$$

$$HSO_2 \rightarrow OH + SO \quad \text{(R5)}$$

$$HOSO \rightarrow OH + SO \quad \text{(R6)}$$

The barriers to reaction are all positive and increase in the order $E_1 < E_2 < E_3$. In addition, the isomer HOSO has a lower zero point energy than HSO_2, which in turn is less than that of H + SO_2. The role of the adducts in the overall reaction has not been fully investigated.

The high barrier to formation even of HSO_2 has limited direct measurements of the H + SO_2 rate coefficient to a single measurement of an upper limit.[1] The rate coefficient for the reverse reaction (OH + SO) has been measured at room temperature using discharge flow by Jourdain et al.[2] and over the temperature range 295−703 K by Blitz et al.[3] using laser flash photolysis. The room-temperature measurements agree well and the flash photolysis experiments show a significant negative temperature dependence, with the rate coefficient decreasing by a factor of 5.5 over the experimental range.

The reaction has also been investigated by theoretical methods. Both Frank et al.[4] and Goumri et al.[5] calculated ab initio potential energy surfaces. Goumri et al.[5] also calculated rate coefficients for the various steps in the mechanism using a RRKM approach. These rate coefficients have subsequently been used in combustion models, notably by Glarborg et al., Alzueta et al., and Dagaut et al.[6−8] in investigations of experiments in flow tube reactors. They proposed that the critical role of H + SO_2 in these systems is in formation of HOSO, which can then react with H to form H_2 and with O_2 to form HO_2. In effect, SO_2 acts as a highly effective third body. Key issues in this proposed mechanism are the rate coefficient for formation of HOSO from H + SO_2 and the thermal stability of

† Part of the special issue "Jürgen Troe Festschrift".
‡ University of Leeds.
§ Accelrys Inc.

10.1021/jp054722u CCC: $33.50 © 2006 American Chemical Society
Published on Web 01/04/2006

HOSO. Hughes et al.[9] also found that H + SO_2 is an important reaction in experiments on low-pressure methane/oxygen/argon laminar flames, seeded with SO_2. The overall reaction H + SO_2 → OH + SO was found to be the major route for destruction of SO_2.

Reaction systems of this sort can show quite complex behavior, which is best investigated via a combination of experimental investigations using, where possible, direct techniques to isolate individual steps, ab initio calculations of the potential energy surface, and master equation (ME) calculations of the interaction between reaction and collisional relaxation based on the potential energy surface. The complexity of the interactions between the various reaction steps and collisional relaxation means that RRKM calculations on individual reaction steps do not provide a complete picture.

Hughes et al.[10] applied a master equation model to H + SO_2, based on the surfaces of Frank et al. and Goumri et al.[4,5] They extracted the rate coefficients for the individual steps by summing the populations of the energy states in each well to obtain species concentrations, and then fitting the time dependent concentration data so generated to analytic solutions of the species concentration time dependence derived from assumed limiting low and high-temperature chemical mechanisms. The data were then fitted to Troe expressions for use in combustion models. This approach is time-consuming and can lead to inaccuracies and ambiguities in assignments. Since then, Klippenstein and Miller [11] have developed a technique whereby the eigenvalues and eigenvectors obtained from the solution of the master equation can be used much more directly and less ambiguously to generate the rate coefficients.

This paper describes an experimental investigation of H + SO_2, using laser flash photolysis, over the temperature range 295−423 K. It represents the first measurement of the rate coefficient for this reaction. These experimental data are then used to refine the ab initio potential energy surface, which in turn is employed in master equation calculations. The rate coefficients for the individual steps are then calculated from the eigenpairs generated from the ME using both the Klippenstein and Miller approach[11] and an alternative method we have derived from the Bartis and Widom approach.[12] A significant issue is the relationship between the ratios of rate constants for forward and reverse reactions and the appropriate equilibrium constants.

The experimental techniques and results are discussed in sections 2 and 3, respectively. In section 4 the master equation model used to analyze the experimental data is developed, refined via fits to the experimental data and used to generate the eigenvalues and eigenvectors for the system. The three eigenvalues of lowest magnitude are what Klippenstein and Miller termed the chemically significant eigenvalues and analysis of their eigenpairs allows determination of the rate coefficients for the individual chemical steps. This analysis, coupled with a classical chemical kinetic analysis permits a detailed interpretation of the eigenvalues, while further analysis of the master equation facilitates interpretation of the mechanisms of these individual steps. In particular, it is shown that, except at very high pressures, the formation of OH + SO occurs from the energized states of HOSO, formed directly from H + SO_2. This observation is compatible with the experimental observation[3] of a pressure independent reaction between OH + SO, that was assumed to lead directly to H + SO_2. The calculations extend this mechanism for the OH + SO reaction by many orders of magnitude in pressure. The resulting chemical kinetic data are parametrized using Troe expressions in section 5, and comparisons with the limited literature data on this reaction is made in section 6. Section 7 provides a brief summary and a list of conclusions.

2. Experimental Section

The laser flash photolysis/laser-induced fluorescence apparatus used to study H atom kinetics has been described previously.[13,14] Briefly, the 248 nm output from a KrF excimer laser (Lambda Physik, LEXtra 50) was used to generate H atoms from the photolysis of CH_3SH.[15] The beam profile of the excimer laser was carefully controlled using an iris of ca. 1 cm diameter. The energy of the photolysis pulses was adjusted using a combination of neutral density filters and the laser voltage, and was measured before entering the reaction cell using a power meter (Scientech 365). The pulsed vacuum ultraviolet (VUV) laser radiation used to excite H fluorescence was generated using the output from an excimer pumped dye laser (Questek vβ 2200/ Lambda Physik FL3002), which was tuned to 364.68 nm (DMQ) and produced up to 20 mJ/pulse. This light was focused using a 10 cm focal length lens into a glass cell containing about 32 Torr of krypton. At the focus a small fraction, on the order of 10^{-6}, of the incident light was tripled[16] to 121.56 nm (Lyman-α) and passed through a magnesium fluoride exit window directly into the reaction cell. The reaction cell was a flanged six-way cross, to which the tripling cell was attached via an O-ring seal that allowed the position of the tripling cell with respect to the reaction cell to be varied. The probe and photolysis beams crossed perpendicularly in the center of the reaction cell and their overlap defined the monitored reaction zone; induced H atom fluorescence was detected at right angles to the plane described by the laser beams. The detection axis flange allowed a Pyrex tube with a magnesium fluoride window at one end to be translated on an O-ring toward the reaction zone. This arrangement allowed variation of the path length of the VUV radiation in the reaction cell. The VUV fluorescence was detected using an Electron Tubes 9423B solar blind photomultiplier tube (PMT) that was purged with nitrogen.

The time delay between the photolysis and probe lasers was controlled using a pulse generator (SRS DG535), with a repetition rate of 2 Hz. The output from the PMT was sampled via a boxcar integrator (SRS 232), digitized and stored on the system control PC, where it was subsequently analyzed. A typical kinetic trace consisted of 400 equally spaced time points, with two samples per point, including several time points before firing the photolysis laser to define the pre-photolysis baseline. Experiments were performed over the temperature range 195−423 K. Above room temperature, cartridge heaters were used to heat the central metal block that surrounds the six-way-cross, and the output of two type K thermocouples mounted above and below the reaction zone were fed to the control box that regulated the power to the heaters. Below room temperature, a dry ice/acetone bath was used to fill the insulated metal box that surrounded the six-way-cross. The temperature of the reaction zone was controlled to better than ±3 K.

The gases used were SO_2 (Air Products 99.5%), He (BOC 99.999%), and CH_3SH (Aldrich 99.5%), which was degassed by freeze pump thaw cycles in liquid nitrogen before diluting in He and storing in 5 L bulbs. Calibrated mass flow meters were used to control the flow of the H atom precursor (CH_3SH), SO_2, and He, the buffer gas. These gases passed into a mixing manifold before introduction into the reaction cell. Pressure in the cell was measured using a capacitance manometer (MKS) and was adjusted between 90 and 600 Torr by throttling the exit valve on the cell The total gas flow at 600

Torr was ~ 5000 standard cubic centimeters per minute (SCCM) ensuring fresh sample in the reaction zone between laser shots, and was varied approximately proportionally to the total pressure.

3. Experimental Results

Photolysis of CH_3SH was observed to produce H atoms, in agreement with Ravishankara et al.[17] who showed that at 248 nm CH_3SH has an absorption cross section of 3×10^{-19} cm^2 and predominantly generates H atoms:

$$CH_3SH \xrightarrow{248\ nm} H + CH_3S \qquad (R7)$$

Production of H using more conventional 193 nm sources was avoided because SO_2 photodissociates at wavelengths below 219 nm.[18] The reaction between H and SO_2:

$$H + SO_2 \rightarrow HSO_2 \qquad (R1)$$

is known to be slow and only a lower limit has previously been assigned to this reaction[1]. H atoms react more rapidly with CH_3SH. Therefore, to observe reaction R1, [CH_3SH] was minimized (typically $\leq 10^{14}$ molecules cm^{-3}). Under these conditions the reaction

$$H + CH_3SH \rightarrow H_2 + CH_3S \qquad (R8)$$

had a removal rate constant of ~200 s^{-1} ($k_8 = 3.5 \times 10^{-11}$ exp(−845/T) cm^3 molecule^{-1} s^{-1} [15]). While reaction R8 was the dominant component of the pseudo-first-order rate constant, k_s, for removal of H atoms in the absence of SO_2, diffusion also contributed significantly to k_s, especially at the lowest pressures and highest temperatures:

$$H \xrightarrow{diffusion} loss \qquad (R9)$$

The detection sensitivity for H in the absence of SO_2 is excellent (<10^9 atom cm^{-3}). This limit mainly reflects interference from scattered VUV light, which totally overlaps the 1.6×10^{-9} s lifetime of the excited state of H;[18] no interference from the fundamental 364.68 nm light was observed with the solar blind PMT. With such detection sensitivity the limit to the quality of the data is the pulse-to-pulse stability of the frequency tripled light, which was measured with a NO ionization cell. Generally, the variability in the probe laser energy was observed to be less than 10%, but the ionization cell behaved erratically when the excimer laser was running. Consequently, the NO ionization cell was not used in the kinetic determinations. Figure 1 shows an example of the quality of the H atom data in the absence of SO_2.

The quality of the data was reduced, however on addition of SO_2. The large absorption cross section of SO_2 at the Lyman α wavelength ($\sigma \sim 2 \times 10^{-17}$ cm^2), coupled with its concentration of up to ~ 4×10^{16} molecules cm^{-3} caused significant absorption of the probe light. To overcome this, the path length between the exit window of the tripling cell and the entrance window of the fluorescence detection was reduced to ca. 2.5 cm by inserting both the tripling and fluorescence tubes into the center of the reaction cell. The reduced quality of the kinetic data in the presence of the highest SO_2 concentration can be discerned from a comparison of Figure 1, parts a and b. Figure 1b also shows that the noise increases with signal size; at these high SO_2 concentrations and low fluorescence intensities, the photon counting regime is approached, where the noise shows Poisson statistics and becomes proportional to the square root

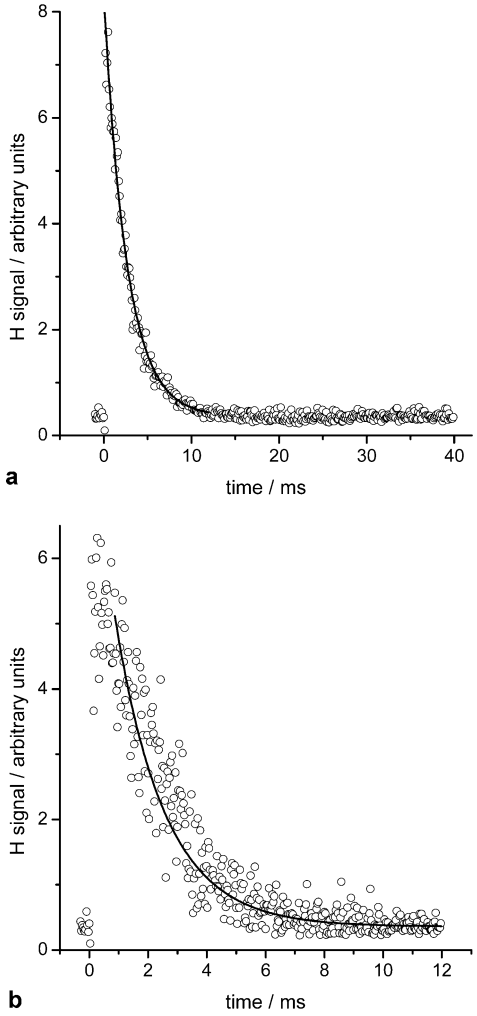

Figure 1. (a) H atom decay profile in the absence of SO_2, $T = 295$ K; total pressure (He) ~ 100 Torr. The trace consists of 400 points with no averaging. (b) H atom decay profile in the presence of ~ 1 Torr SO_2, $T = 295$ K; total pressure (He) ~ 300 Torr. Both traces consist of 400 points with no averaging.

of the signal. At these higher concentrations of SO_2, Poisson weighting was applied; it only had a significant effect on the returned rate constant, compared to constant weighting, at higher [SO_2]. At the highest [SO_2] the Poisson weighting returned a rate constant ca. 25% higher.

Addition of SO_2 increased the removal of H from the system, and the H atom time profiles were observed to follow single exponential behavior:

$$[H] = [H]_0 \exp(-k'_1 t) \qquad (E1)$$

where $[H]_0$ is the initial H atom concentration and $k'_1 = k_1[SO_2] + k_s$ ($[H] \ll [SO_2]$). A set of H atom kinetic traces were recorded in the presence of SO_2, where [SO_2] $\leq 4 \times 10^{16}$ molecules cm^{-3}, and subsequently analyzed by fitting equation (E1) to the data, weighted statistically, to yield k'_1. A plot of the pseudo-first-order rate constant, k'_1, vs [SO_2] should yield a straight-line whose slope is equal to the H + SO_2 rate constant, k_1, an example of which is shown in Figure 2a. However, it was found that the apparent rate constant $k_{1,apparent}$, increased with the excimer photolysis energy. The source of this effect was characterized by a series of the experiments where the laser energy was carefully adjusted over ca. an order of magnitude.

While SO_2 does not directly photolyze at 248 nm it does absorb ($\sigma_{248\ nm} \sim 7 \times 10^{-20}$ cm^2 [18]). Previous studies [19−21] on

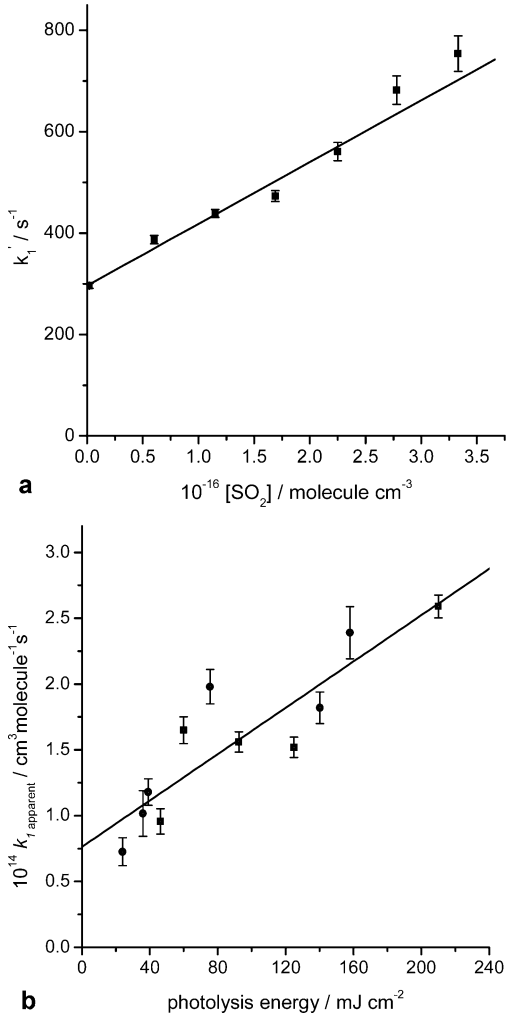

Figure 2. (a) Plot of k_1' vs [SO_2] at 295 K and 400 Torr total pressure. The slope is equal to $k_{1apparent}$. The error bars are from the first order fits to traces such as that shown in Figure 1b) and are purely statistical. (b) Plot of $k_{1apparent}$ vs laser fluence: (●) 300 Torr total pressure at 295 K; (■) 100 Torr total pressure at 195 K.

the photochemistry of SO_2 between 240 and 400 nm have identified the following mechanism:

$$SO_2 + h\nu \rightarrow {}^1SO_2\,({}^1B_1) \qquad \text{(R10a)}$$

$$\rightarrow {}^3SO_2\,({}^3B_1) \qquad \text{(R10b)}$$

$${}^1SO_2 + SO_2 \rightarrow SO_2 + SO_2 \qquad \text{(R11a)}$$

$${}^3SO_2 + SO_2 \rightarrow SO_3 + SO \qquad \text{(R11b)}$$

While a more complete mechanism includes additional steps these are of only minor importance. Cox[20] determined a value of 0.004 for quantum yield for SO_3 formation, ϕ_{SO_3}, with broad band (290−400 nm) irradiation of pure SO_2; little or no pressure dependence was observed. In the present experiments it would appear that 248 nm photolysis of SO_2 produces SO_3; use of $\sigma_{248\ nm}$ and ϕ_{SO_3} gives [SO_3] ≤ 10^{12} molecules cm^{-3}. The SO_3 was formed on a time scale of <100 μs under the experimental conditions employed here.[20]

Experiments were performed where the bimolecular rate constant $k_{1,apparent}$ was determined as the photolysis energy was varied over the range 20−220 mJ $pulse^{-1}$. This procedure was performed at 300 Torr at room temperature and 100 Torr at 195 K, and the results are summarized in Figure 2b, from which

TABLE 1: Rate Coefficients for H + SO_2 Obtained from Plots of k_1 vs [SO_2] with the Contribution from the Pulse Energy Dependence Subtracted via Equation E3[a]

T/K	10^{18} [He]/molecule cm^{-3}	10^{15} k_1/cm^3 molecule^{-1} s^{-1}
295	3.37	2.26 ± 1.88
295	6.64	3.82 ± 1.68
295	9.97	5.83 ± 2.09
295	13.1	7.56 ± 1.84
295	17.7	9.80 ± 2.14
295	23.0	12.3 ± 2.02
363	2.73	2.95 ± 1.68
363	7.93	7.97 ± 2.44
363	18.3	15.8 ± 1.93
423	5.02	8.98 ± 3.41
423	9.22	12.3 ± 3.06
423	15.7	16.8 ± 3.10

[a]Errors represent 2σ.

it can be discerned that the $k_{1,apparent}$ has a linear dependence on photolysis energy. The dependence on photolysis energy suggests that H reacted with photoproducts produced in the system, possibly via the following reaction:

$$H + SO_3 \rightarrow OH + SO_2 \qquad \text{(R12)}$$

If reaction R12 is responsible for the photolysis pulse energy dependence, then k_{12}, must be close to gas-kinetic. There are no previous experimental determinations of k_{12} but it is used in the model by Glarborg et al.[8] on the effect of SO_2 on CO oxidation. The value of k_{12} at 300 K from this model is $\sim 10^{-15}$ molecules cm^3 s^{-1} and is based on a QRRK estimate with a barrier to reaction. If reaction R12 is indeed responsible for the pulse energy dependence, then the barrier to reaction must be very small. The reaction is ~80 kJ mol^{-1} exothermic.

An alternative explanation is reaction between H and $^3SO_2$. In an investigation of OH + SO_2, Blitz et al.[14] observed that the OH decay had a contribution which was dependent on the laser photolysis energy, which they assigned to the reaction OH + $^3SO_2$. This mechanism is unlikely under the experimental conditions employed here, because $^3SO_2$ is too short-lived.

Although the mechanism of the pulse energy dependence is not fully explained, it is clear that $k_{1,apparent}$ increases linearly with energy and that the most reasonable empirical approach to the determination of k_1 is to extrapolate to zero energy. Figure 2b gives

$$k_1 = k_{1,apparent} - (8.8 \times 10^{-17}\ cm^3\ s^{-1}\ mJ^{-1}\ cm^2)F \qquad \text{(E2)}$$

where F is the excimer laser fluence in mJ cm^{-2} and 8.8×10^{-17} cm^3 s^{-1} mJ^{-1} cm^2 is the average slope in Figure 2b which shows little if any dependence on temperature. Typically, k_1 was determined using 50 mJ/pulse and the results are summarized in Table 1. This photolysis energy provided sufficient signal for good kinetics analysis, while ensuring that the effective contribution from R12 was $\leq 5 \times 10^{-15}$ cm^3 molecule^{-1} s^{-1}. The correction ranged from 20 to 70%.

Owing to the difficulty in performing the photolysis energy dependent experiments, we have assigned a 30% uncertainty in the slope of the plot in Figure 2b, which corresponds to 1.5 $\times$ 10^{-15} cm^3 molecule^{-1} s^{-1} at 50 mJ/pulse. This uncertainty was propagated in the determination of k_1 via eq E2. Table 1 shows that k_1 increases with both pressure and temperature, as would be expected for an association reaction with a substantial energy barrier of 8.9 kJ mol^{-1} as calculated by Goumri et al.[5] The maximum temperature at which experiments could be performed was limited by the experimental design of the tripling

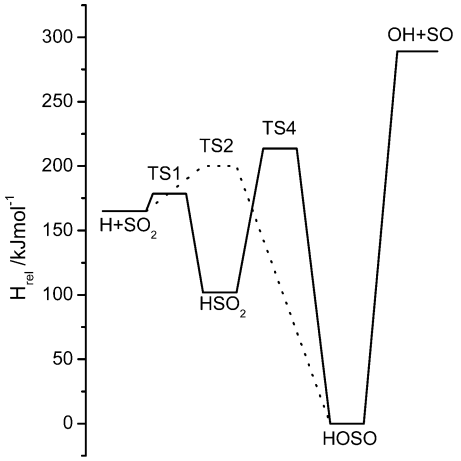

Figure 3. Potential energy surface for H + SO_2. The transition state energies are taken from Goumri et al. and the energies of the stable species from Frank et al. The transition state linking HOSO and OH + SO is TS6.

cell and the sealant used for the MgF_2 window. This temperature was unfortunately too low to observe back reaction from HSO_2 via reaction (R − 1).

4. Master Equation Modeling and Analysis

4.1. Master Equation Model. In previous work,[10] a master equation (ME) model was developed for the H + SO_2 system based on the ab initio studies of Frank et al.[4] and Goumri et al.[5] Figure 3 shows the potential energy surface in which the two intermediate isomers, HSO_2 and HOSO, are connected by the transition state TS4. HSO_2 and HOSO are connected to the reactants via the transitions states TS1 and TS2 respectively while HOSO can dissociate to give OH and SO, via transition state TS6. The energies of the transition states TS1, TS2, and TS4 were taken from Goumri et al.,[5] while the energies of the stable species were taken from Frank et al.[4]

The ME approach has been discussed in detail elsewhere[22,23] and only a brief account is given here. The general form of the ME for this system is

$$\frac{d\mathbf{p}}{dt} = \mathbf{M}\mathbf{p} \qquad \text{(E3)}$$

where **p** is a vector, describing the time evolution of the population of the microcanonical rovibrational states and the matrix **M** is the collision matrix, which describes the rate at which population is transferred between states due to collisional activation/deactivation and reaction. To understand the evolution of the system it is necessary to solve eq E3, and this was done using the standard energy graining and diagonalization approach discussed previously.[10] The population vector was constructed by concatenating the energy grained population vectors of HSO_2 and HOSO rovibrational states. The grain size used was 100 cm^{-1}. All energies were measured relative to the zero-point energy of HOSO, being the lowest energy point on the surface. A maximum energy range of 50000 cm^{-1} was used, and so HOSO was represented by 500 grains and HSO_2 by 414 grains. The number of states in each grain and their mean energy were calculated by convolving classical rotational densities of states with vibronic states obtained using the Beyer−Swinehart algorithm. An extra element was then added to represent the population of H atoms; as in the experiment, SO_2 was in excess so that the kinetics of H + SO_2 were pseudo first order. The energy transfer terms were modeled using an exponential down model in combination with a Lennard-Jones collision frequency.

The structure of the matrix **M** reflects the topology of the potential energy surface. The two main blocks on the leading diagonal represent the energy transfer between rovibrational states of HSO_2 and HOSO in addition to reactive loss to other species. The off diagonal blocks of **M** represent reactive formation from another species. The microcanonical rate coefficients for reaction via transition states TS1, TS2 and TS4, were calculated using RRKM theory, subject to the constraint of detailed balance. It is important to recognize the relationship between the six sets of rate coefficients for reaction over these transition states when implementing a ME solution: in the absence of reactive loss through the dissociation of HOSO to OH and SO, the system must come to a stable equilibrium consistent with thermodynamics. The equilibrium constants, given by ratios of canonical rate coefficients, must be internally consistent, such that the specification of any two automatically specifies the third. This constraint was built into the model and tested by temporarily switching off the HOSO → OH + SO dissociation channel and examining the solution at long times to ensure that population is conserved, that there were no spurious loss terms and that the ratios of concentrations were consistent with the thermodynamics of the system. At very long times, some loss was observed resulting from the use of finite precision arithmetic; it occurred in a time region far removed from that of chemical interest.

The dissociation of HOSO to give OH and SO proceeds over a barrierless potential. One approach to calculating the microcanonical rate coefficients for such a reaction would be to use a variational technique to locate TS6 as a function of energy. Such an approach requires considerable information on the potential energy surface, which is not available at present. Consequently mircocanonical rate coefficients where obtained using the inverse Laplace transform method,[24,25] based on the measurements of the limiting high-pressure rate coefficient for OH + SO.[3]

The above scheme was implemented using the LAPACK[26] suite of linear algebra routines to diagonalize the collision matrix. As with previous studies[23] difficulties were encountered when calculations were performed for low temperatures (<1000 K), because the ratio of the eigenvalue of smallest magnitude to that of largest magnitude exceeded machine precision. As a result, essential detail was lost on the eigenvalues of smallest magnitude, which are most important in determining the chemical evolution of the system. To make progress in the analysis of the present system the calculations were repeated using quadruple precision arithmetic which allowed the whole system to be analyzed at temperatures of 200 K and above.

4.2. Fits to Experimental Data. The low-temperature experimental rate coefficients for reaction R1, H + SO_2 → HSO_2, reported in this paper, were used to optimize the potential energy surface with respect to the barrier height of TS1 and the well depth of HSO_2, in addition to allowing a refinement of the collisional energy transfer parameter, $\langle\Delta E\rangle_{down}$. The low temperature conditions in the experiments allowed a simplified potential energy surface to be employed (confirmed in the more detailed calculations described below), consisting solely of H + SO_2 and HSO_2 connected via TS1. The master equation of this reduced system was solved in quadruple precision. It is conservative and so has a zero eigenvalue; the forward and reverse rate coefficients are related to the nonzero eigenvalue of smallest absolute magnitude by eq E4.

$$|\lambda| = k_1[SO_2] + k_{-1} \quad \text{(E4)}$$

Under the experimental conditions, $[SO_2] \gg [H]$, the forward reaction dominates, and so k_1 can be determined from the value of $|\lambda|$ returned from the master equation analysis. Satisfactory fits to the experimental data required a small increase in the barrier height of 4.7 to 13.6 kJ mol^{-1}, with $\langle \Delta E \rangle_{down}$ for the helium bath gas set at 95 cm^{-1}. Since the reverse dissociation of HSO_2 was not observed experimentally, the results are comparatively insensitive to the well depth, which could not, in consequence, be optimized. The results are shown in Figure 4 for 295, 363, and 423 K. Table 2 summarizes the rotational constants, vibrational frequencies, and relative energies of the intermediates and transition states which were then used in the full master equation model.

4.3. Determination of Phenomenological Rate Coefficients from ME Results. In our previous paper,[10] the ME model results for the time evolution of the species concentrations were fitted to analytical solutions derived from the limiting low and high-temperature approximations for reactions R1−R3 and R6. (see scheme in section 1). Reactions R4 and R5 were considered, but they were rejected as unimportant after a preliminary analysis of the system by numerical integration Best fit rate coefficients were obtained as functions of T and p over the temperature range 300−2000 K This procedure is not entirely satisfactory owing to the time-consuming and tedious nature of setting up the analysis and the fact that the analytical solutions are only strictly valid at the extremes of the temperature range (see below).

Since then Klippenstein and Miller[11] have demonstrated how phenomenological rate coefficients can be extracted from the eigenvalues and eigenvectors of the collision matrix of the master equation. The basis of the approach is the construction of rate equations for macroscopic concentrations that describe the evolution of a species at the initiation of reaction, and in particular for the case when all the initial population density is accumulated in one given species. Then, by calculation of sums over appropriate ranges and combinations of the eigenvalues and eigenvectors, rate coefficients for all the possible chemical reactions that the reactant could undergo are computed. For example, in the H + SO_2 system depicted in Figure 3, obtaining the master equation solution with the initial condition of reactants being H + SO_2 allows rate coefficients to be directly obtained for the three possible chemical reactions R1, R2, and R3. By altering the initial condition such that the initial reactant is a normalized Boltzmann distribution of HSO_2, rate coefficients for $HSO_2 \rightarrow H + SO_2$ (R−1), $HSO_2 \rightarrow$ HOSO (R4), and $HSO_2 \rightarrow$ OH + SO (R5) are obtained. For the case when the initial reactant is HOSO, rate coefficients for its three possible reactions (R−2, R−4, and R6) are determined. In contrast to the more limited information that can be obtained with considerable effort using the species profile fitting method, the entire set of rate coefficients in the system can now be directly computed with a fraction of the effort.

Klippenstein and Miller,[11] also discussed an earlier approach by Bartis and Widom[12] for the extraction and interpretation of phenomenological rate coefficients. Bartis and Widom derived a set of macroscopic rate equations from the master equation by integrating over microscopic energy states and showed that the evolution of a linear system on the time scale of reaction, subject to certain restrictions, is accurately described by equations that are identical in form to phenomenological rate equations. They deduced formulas for the macroscopic rate coefficients that obey detailed balance and are not expressed solely in terms of the properties of one species or another but by the properties of the whole system. The validity of these conclusions is subject to two restrictions: (i) the system is conservative, so that there is no net loss of population density from the system, or equivalently, all the eigenvalues are negative except one which is identically zero; (ii) the eigenvalue spectrum can be separated into two parts, one part describing the fast energy transfer modes and the other containing the chemically significant eigenvalues (CSE),[11] which include the zero eigenvalue. In general for the phenomenological equations to be valid the number of CSE must be equal to the number of macroscopic species that comprise the system. They must also be well separated in magnitude from the eigenvalues that relate to collisional relaxation.

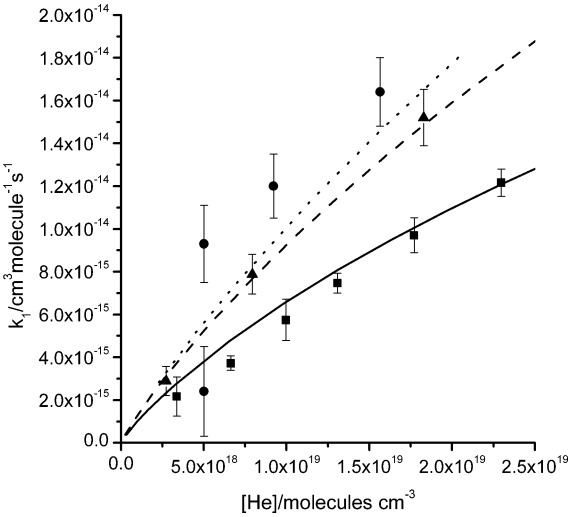

Figure 4. Experimental data for k_1 and fits generated from the master equation model, by varying the energy of TS1 and $\langle \Delta E \rangle_{down}$: (■) T = 295 K; (▲) T = 363 K; (◆) T = 423 K.

In the present analysis the restriction that the system be conservative (i.e., has an eigenvalue of zero) was dropped, and the Bartis−Widom approach was applied directly. Klippenstein and Miller[11] also examined this approach but found it necessary to expand the rate coefficient matrix with terms that represented the sink term species. In the analysis that follows, this expansion is not required.

Figure 5 shows, for the present system, the lowest four eigenvalues at a pressure of 1 atm and as a function of temperature. These eigenvalues are labeled λ_1, λ_2, λ_3, and λ_4 and have the relative magnitudes, $|\lambda_1| < |\lambda_2| < |\lambda_3| < |\lambda_4|$. The eigenvalues are well separated below 1000 K, but λ_3 and λ_4 have very similar magnitudes above 1200 K. The importance of this observation will be discussed later.

To extract the phenomenological rate coefficients for the H + SO_2 system, from the eigenvalues shown in Figure 5 and associated eigenvectors, both the approach described by Klippenstein and Miller and one based on that of Bartis and Widom were used. Satisfactory rate coefficients where obtained from both approaches, but as the Bartis−Widom (BW) approach was slightly easier to implement and because it might (as pointed out by Klippenstein and Miller) be regarded as a more fundamental approach, it was used in the remainder of the study.

A derivation of the phenomenological equations from the ME is given, for convenience, in Appendix A. It differs slightly from that given by either Bartis and Widom[12] or Klippenstein and Miller,[11] in that the resulting canonical rate coefficients explicitly do ***not*** depend on the initial distribution. (Klippenstein and Miller noted the apparent dependence on initial distribution in

TABLE 2: Relative Energy, Rotational Constants, and Vibrational Frequencies of Reactants, Products, Intermediates, and Transition States

	H_{rel}/kJ mol^{-1}	rotational constants/cm^{-1}	vibrational frequencies/cm^{-1}
H + SO_2	165	2.016, 0.345, 0.295	518, 1151, 1362
HSO_2	102	1.703, 0.3, 0.263	411, 777, 1027, 1094, 1578, 2284
HOSO	0	1.14, 0.309, 0.243	183, 336, 722, 991, 1283, 3493
OH + SO	289	18.87, 0.95	3725, 1396
TS1	178.6	1.22, 0.321, 0.275	347, 358, 517, 1177, 1381
TS2	199.9	1.506, 0.295, 0.256	407, 639, 854, 1216, 2191
TS4	213.6	1.486, 0.299, 0.261	298, 500, 609, 1218, 1527

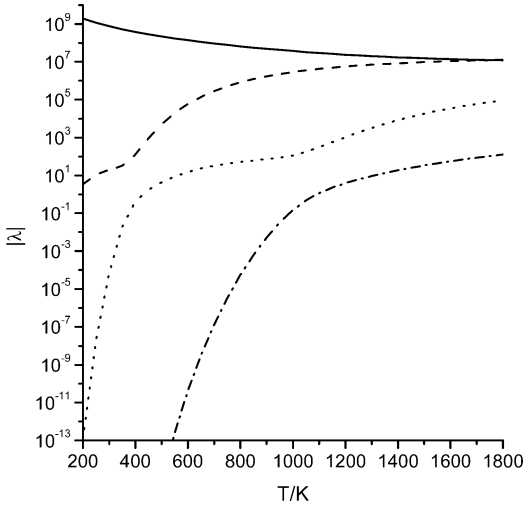

Figure 5. Four lowest absolute eigenvalues as a function of temperature at 1 atm: (- · -) $|\lambda_1|$; (···) $|\lambda_2|$; (- -) $|\lambda_3|$; (—) $|\lambda_4|$.

their analysis and stated that the "The energy-relaxation eigenpairs always establish the appropriate distribution prior to reaction taking place.") The present approach gives the same principal result, the equations of motion describing the macroscopic evolution of the system, which are given by

$$\frac{d\mathbf{r}}{dt} = \mathbf{Z}\Lambda'\mathbf{Z}^{-1}\mathbf{r} = \mathbf{K}_r\mathbf{r} \qquad \text{(E5)}$$

where **r** is a vector whose elements are the concentrations of the macroscopic species, which for the present system is

$$\mathbf{r} = \begin{pmatrix} [HSO_2] \\ [HOSO] \\ [H] \end{pmatrix} \qquad \text{(E6)}$$

Λ' is a diagonal matrix of the CSE and the **Z** matrix is formed from the elements of the eigenvectors as outlined in Appendix A. These equations apply to a system whose collision matrix eigenvalues are all negative (has an infinite sink).

The matrix $\mathbf{K}_r$ that appears after the second equality in eq E5 represents the rate coefficient matrix for evolution of the macroscopic system. Expressions for these rate coefficients were derived by Bartis and Widom. Here a more pragmatic approach was adopted, the elements of $\mathbf{K}_r$ are identified with the elements of the corresponding rate coefficient matrix obtained from the phenomenological rate equations. For the present system this has the following form:

$$\mathbf{K}_r = \begin{pmatrix} -k_{-1} - k_4 - k_5 & k_{-4} & k_1 \\ k_4 & -k_{-4} - k_{-2} - k_6 & k_2 \\ k_{-1} & k_{-2} & -k_1 - k_2 - k_3 \end{pmatrix} \qquad \text{(E7)}$$

This matrix exhibits two important features. The first of these is that there are rate coefficients, k_3, k_5, and k_6, for formation of OH + SO (and so loss of population density from the system) for each species. While the only transition state leading to OH + SO (TS6) links these products to HOSO, our previous investigation had shown that the master equation data could not be fitted for some conditions (most notably at high temperature and low pressure) if the direct bimolecular reaction (reaction R3) were not included. Reaction occurs from the energized states of HOSO, following formation from H + SO_2, without collisional stabilization to HOSO. This behavior mirrors that observed by Miller and Klippenstein for $C_2H_5 + O_2$.[27] For completeness k_5 was added and represents the concerted isomerization and dissociation of HSO_2. The second important feature is that in the absence of dissociation to form OH + SO ($k_3 = k_5 = k_6 = 0$) the columns of **Kr** sum to zero as they must for a conservative system. While this latter feature imposes some restriction on the identity of the elements thereof, there will always remain a degree of arbitrariness about the assignment of rate coefficients for a system which has one or more infinite sinks. This issue will be reexamined in section 4.6

With the assignment in eq E7, the rate coefficients were extracted from the eigenvalues and eigenvectors of the collision matrix. These rate coefficients were tested by integrating eq E5 and comparing those results with the results for the master equation. In almost all cases the agreement was found to be excellent for all times except the very short times, which correspond to the energy relaxation period. Some cases did, however, show divergence. This occurred at high temperatures (1750K for pressure of 1 atm) where the separation between chemically significant and energy relaxation eigenvalues is less marked, and indeed where the two sets tend to overlap. In these circumstances eq E5 no longer describes the evolution of the chemical system, and consequently, it is not possible to write a set of phenomenological equations and extract rate coefficients.

4.4. Rate Coefficients from the Bartis and Widom Analysis of the Master Equation Results. Rate coefficients for all the possible reactions in the system were generated with the Bartis and Widom method, for a temperature range of 200−1700 K and a pressure range from 10^{-3} to 10^{6} atm. Examples of these plots are shown in Figure 6a−e. The rate coefficients for reactions R1 and R2 show the standard pressure dependent form for association or dissociation reactions, increasing to a high-pressure limit. Their reverse reactions show a similar pressure dependence and their rate coefficients can be determined via the equilibrium constants. The fits shown are for a standard Troe treatment,[28] and the best fit parameters are discussed in section 5. k_3 shows the inverse behavior, with a low-pressure asymptote and a decrease in the rate coefficient as the pressure increases. This type of behavior is typical of a reaction in which dissociation (in this case to OH + SO) competes with stabilization (to HOSO). The rate coefficients for reactions R4 and R6 show a more complex, bimodal behavior, which will be discussed in section 4.7.

4.5. Relationship of Chemically Significant Eigenvalues to Rate Coefficients. The interpretation of the rate coefficients and of the behavior of the whole system as a function and temperature and pressure, is best achieved through a comparison of the three chemically significant eigenvalues, λ_1, λ_2, and λ_3, with the rate coefficients for the individual reactive steps. A useful approach is to use high and low-temperature analytic solutions for these eigenvalues, based on the solution to the system defined by the chemical scheme given in the Introduction and by eq E7. These analytic solutions, and their dependence on the rate coefficients for the various chemical steps, can then be compared with the eigenvalues from the master equation over the whole range of pressure and temperature.

At low temperatures (<1000 K), reactions R1, R−1, R2, and R−2 dominate the system, which is consequently conservative. As a result, stoichiometry can be used to reduce the system to two variables and to two nonzero eigenvalues, λ_3 and λ_2, which are given by

$$\lambda_{2,3} = (-p \pm \sqrt{p^2 - 4q})/2 \qquad \text{(E8)}$$

where

$$p = k'_1 + k_{-1} + k'_2 + k_{-2}$$

and

$$q = k'_1 k_{-2} + k_{-1}(k'_2 + k_{-2})$$

where $k'_1 = k_1[SO_2]$ and $k'_2 = k_2[SO_2]$. k_1, $k_{-1} \gg k_2$, k_{-2} and the eigenvalues are well separated, so that, to a good approximation

$$|\lambda_3| \approx k'_1 + k_{-1} + k'_2 + k_{-2} \approx k_1[SO_2] + k_{-1} \qquad \text{(E9)}$$

and

$$|\lambda_2| \approx \frac{k'_1 k_{-2} + k_{-1}(k'_2 + k_{-2})}{k'_1 + k_{-1}} = k_{-2} + \frac{k'_2}{1 + K_1[SO_2]} \qquad \text{(E10)}$$

where $K_1 = k_1/k_{-1}$.

At higher temperatures, $k_{-1} \gg k_1[SO_2]$, so that the concentration of HSO_2 is insignificant and the system reduces to reactions R2, R−2, R3, and R6. The solutions for $\lambda_{1,2}$ take the form shown in eq E8, with

$$p = k'_2 + k_{-2} + k'_3 + k_6$$

and

$$q = k'_2 k_6 + k'_3(k_{-2} + k_6)$$

k'_2, $k_{-2} \gg k_3$, k_6, giving the following solutions to $\lambda_{1,2}$ to good approximation:

$$|\lambda_2| \approx k'_2 + k_{-2} + k'_3 + k_6 \approx k_2[SO_2] + k_{-2} \qquad \text{(E11)}$$

$$|\lambda_1| \approx \frac{k'_2 k_6 + k'_3(k_{-2} + k_6)}{k'_2 + k_{-2}} \approx \frac{k_3[SO_2] + k_6 K_2[SO_2]}{1 + K_2[SO_2]} \qquad \text{(E12)}$$

where $K_2 = k_2/k_{-2}$.

These approximate analytic solutions for the eigenvalues can be used to guide the interpretation of the three chemically significant eigenvalues derived from the master equation, using the relationships shown in eqs E9−E12 and the rate coefficients determined from the modified Bartis−Widom approach.

Figure 7a shows a comparison between the $|\lambda_3|$ and the rate coefficients $k_1[SO_2]$ and k_{-1} for 1 atm. At low T, $k_1[SO_2]$ dominates, while at high T $|\lambda_3| = k_{-1}$ to a good approximation. Over the whole temperature range, $k_1[SO_2] + k_{-1}$ provides an excellent representation of $|\lambda_3|$ and is, from a practical perspective, indistinguishable from the full solution given in eq E8 at all pressures and temperatures investigated. Thus $|\lambda_3|$ relates to relaxation about TS1. Its close relationship to k_{-1} for $T > 600$ K and the small value of K_1 at the higher temperatures demonstrate that HSO_2 is unimportant under these conditions, because of its rapid dissociation to regenerate H + SO_2. Note however that at temperatures above 1200 K, $\lambda_3 \approx \lambda_4$ which may compromise this analysis, giving effective rate constants derived from a mixture of these two eigenvalues. From a practical perspective, this is not an important issue, because HSO_2 is so rapidly dissociated at these temperatures that reactions R1 and R−1 contribute little to the overall reactive system at realizable $[SO_2]$.

Figure 7b compares the ME solution for $|\lambda_2|$ and the relevant rate coefficients at 1 atm pressure. At low T, eq E10 applies. Under these conditions, $K_1[SO_2]$ is significant, while $k_2[SO_2] \gg k_{-2}$, so that $|\lambda_2| = k_2/K_1$. The eigenvalue is determined by the rate of reaction (R2), which is limited by the fraction of the H atom concentration that is tied up as HSO_2. At higher temperatures, $K_1[SO_2] \ll 1$, HSO_2 plays a negligible role in the reaction, and at this pressure, $|\lambda_2|$ from both (E10) and (E11) approaches $k_2[SO_2] + k_{-2}$. Figure 7b shows that, except at very low temperatures, the rate constant for relaxation to equilibrium, $k_2[SO_2] + k_{-2}$, provides an accurate representation of the eigenvalue from the master equation analysis over the whole temperature range studied, with the first term dominating at lower temperatures and the latter term at higher temperatures. This behavior persists at the higher pressures investigated; at 1×10^{-3} atm, however, there is evidence that k_3 makes a significant contribution at intermediate temperatures (Figure 7c) and cannot be neglected from eq E11. As shown above, k_3 is independent of pressure at low p, while k_2, k_{-2}, and k_6 all increase with p, so that the contribution of reaction R3 to λ_2 is greatest under low-pressure conditions. Even when k_3 does make a significant contribution, the fuller representations of the eigenvalue (eq E8 in its low and high temperature forms) provides an accurate representation of the eigenvalue from the master equation (see Figure 7c). Thus, for the most part, λ_2 relates to passage over TS2 but with some evidence of a contribution to passage over TS6 following formation of energized HOSO via H + SO_2, at low pressures and high temperatures.

Parts d and e of Figure 7 show the temperature dependence of $|\lambda_1|$ at 1 atm and at 1×10^6 atm, respectively. In both cases, the high-temperature version of the analytic solution shows good agreement with the appropriate master equation eigenvalue. At 1 atm, k_6 can be neglected, and the approximate solution (eq E12) reduces to $k_3[SO_2]/(1 + K_2[SO_2])$. The formation of OH + SO is dominated by reaction R3 with a modification at low temperatures, where $K_2[SO_2] \gg 1$, to account for the fraction of H tied up as HOSO. At 1×10^6 atm, formation of OH + SO from stabilized HOSO (reaction R6) dominates, thus (E12) now simplifies to $k_6 K_2[SO_2]/(1 + K_2[SO_2])$ in which k_6 is modified at high temperatures where $K_2[SO_2] \ll 1$ to provide the fraction of HOSO in equilibrium with H.

4.6. Comparison of Rate Coefficient Ratios and Equilibrium Constants. The H + SO_2 system is not conservative, and it is of interest to examine how well rate constant ratios agree with equilibrium constants.

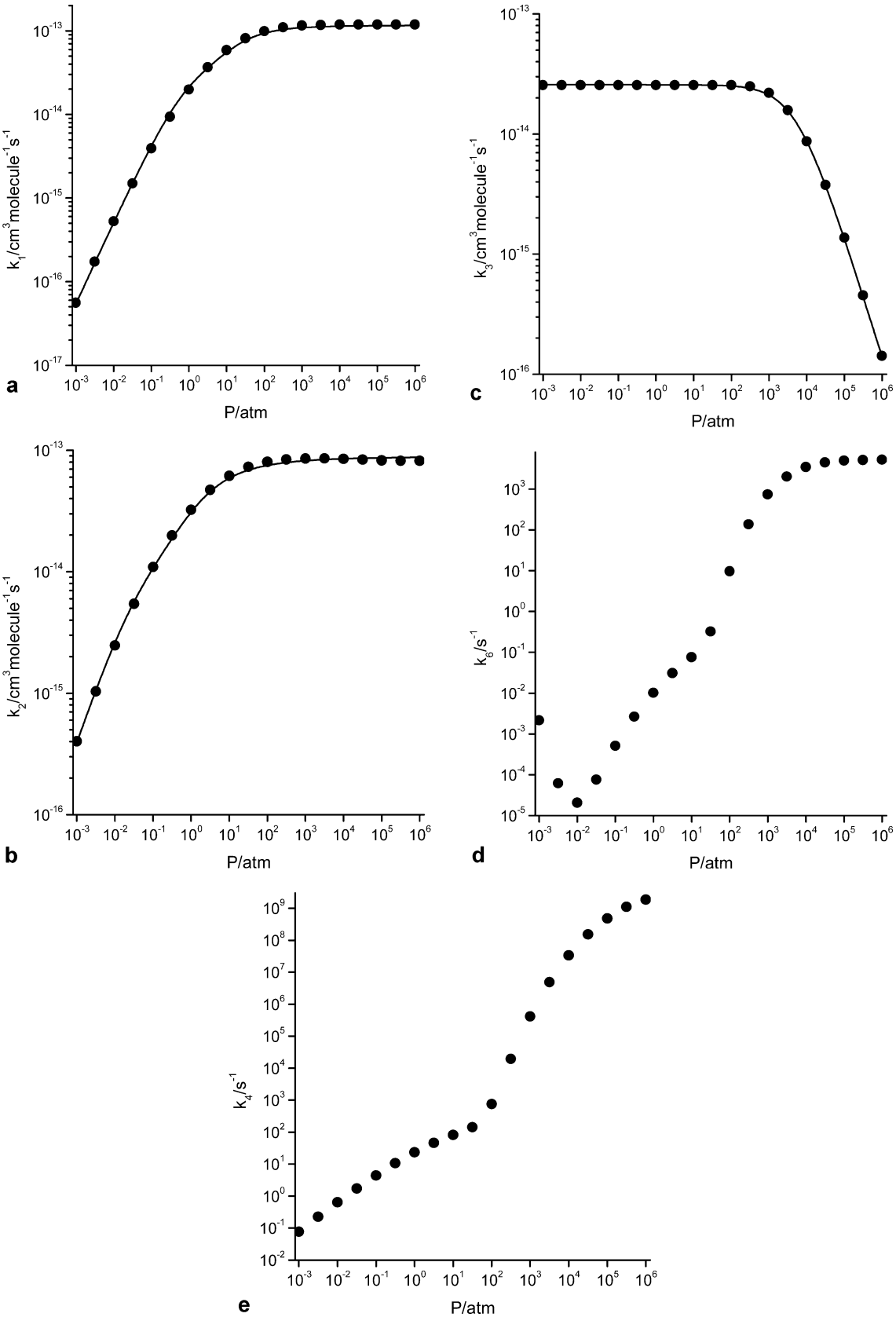

Figure 6. Rate coefficients for reaction steps as a function of pressure: (a) k_1 at 300 K; (b) k_2 at 700 K; (c) k_3 at 1450 K; (d) k_6 at 1450 K; (e) k_4 at 1450 K. Troe (eq E14) fits are shown in parts a and b and a modified Troe fit (eq E17) in part c. Fits were not possible for k_4 and k_6.

(i) k_1 and k_2. These reactions do not lead to loss from the H + HSO_2 + HOSO system. Comparisons between ratios of forward and reverse rate coefficients and equilibrium constants shows agreement for reactions R1 and R−1 and reactions R2 and R−2, to better than 0.001%.

(ii) k_3 and k_6. These reactions lead to loss from the system, with reaction R3 dominating below ∼1000 atm and reaction R6 above ∼10000 atm. The calculations were performed for $[SO_2] = 1 \times 10^{15}$ cm^{-3}, but this conclusion is unaffected by changes in $[SO_2]$. The reactions only become significant (time

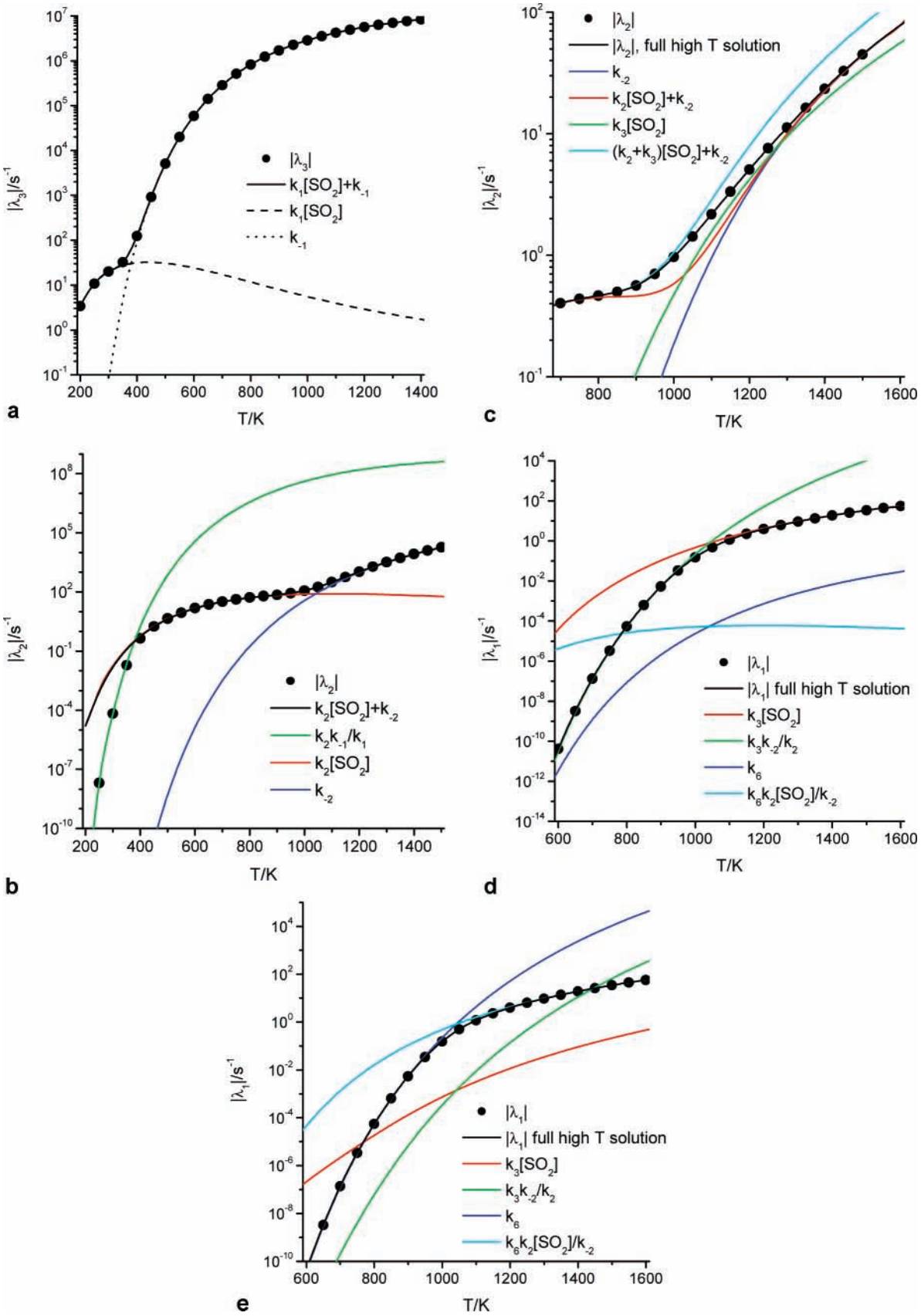

Figure 7. Relationships between eigenvalues and combinations of rate coefficients, as a function of temperature: (a) $|\lambda_3|$ at 1 atm; (b) $|\lambda_2|$ at 1 atm; (c) $|\lambda_2|$ at 1×10^{-3} atm; (d) $|\lambda_1|$ at 1 atm; (e) $|\lambda_1|$ at 1×10^{6} atm.

scales < 1 s) at temperatures greater than ~900 K. The reverse reaction, OH + SO, shows interesting characteristics. It is pressure independent, as would be expected for an association reaction with a barrier for dissociation to H + SO_2 well below the reactant energy asymptote. It also has a strong negative temperature dependence. A fit directly to the experimental data gave $k = 8.3 \times 10^{-11}$ $(T/295\ \mathrm{K})^{-1.35}$ cm^3 molecule^{-1} s^{-1};[3] slightly different values ($A = 9 \times 10^{-11}$ cm^3 molecule^{-1} s^{-1}

TABLE 3. Derived Rate Coefficients from Fitting Troe-Type Expressions (Equations E14 and E17) to the Output of the Master Equation Analysis[a]

	low-pressure limit			high-pressure limit			
reaction	A	n	E/K	A	n	E/K	Troe parameters A, T^{***}, T^{*}
$H + SO_2 \rightarrow HSO_2$,[b] k_1	5.42×10^{-30}	−5.19	2271	7.66×10^{-12}	1.59	1244	0.390, 167, 2191
$HSO_2 \rightarrow H + SO_2$,[b] k_{-1}	$k_{-1} = k_1/K_{eq,1}$ ($K_{eq,1} = 3.87 \times 10^{-25}(T/300)^{0.28} \exp(8189/T)$)						0.390, 167, 2191
$H + SO_2 \rightarrow HOSO$,[c] k_2	3.15×10^{-26}	−6.14	5573	4.30×10^{-12}	1.63	3693	0.283, 272, 3995
$HOSO \rightarrow H + SO_2$,[c] k_{-2}	$k_{-2} = k_2/K_{eq,2}$ ($K_{eq,2} = 1.81 \times 10^{-24}(T/300)^{0.576} \exp(20197/T)$)						0.283, 272, 3995
$H + SO_2 \rightarrow OH + SO$,[d] k_3	4.51×10^{-8}	−2.30	15 582	1.11×10^{9}	2.77	10 491	1.00, 272, 27617

[a] Each rate coefficient is of the form $k = A \times (T/300)^n \times \exp(-E/T)$. Units: k_1, k_2 are cm^6 $molecule^{-2}$ s^{-1} and cm^3 $molecule^{-1}$ s^{-1} for low and high pressure, respectively; K_{eq} is cm^3 $molecule^{-1}$, and k_3 values are cm^3 $molecule^{-1}$ s^{-1} and s^{-1} for the low and high pressure, respectively. [b] Fitted using E14 over the range 200−1000 K. [c] Fitted using E14 over the range 300−1700 K. [d] Fitted using E17 over the range 900−1800 K.

and the exponent $n = -1.2$) were used in the present analysis, based on a master equation analysis of OH + SO, fitting the rate parameters using an inverse Laplace transform approach. A comparison between the value calculated for k_6, at high T and p (1600 K and 1×10^8 atm) shows a 8% difference between the value returned for k_6 and that calculated from the association rate coefficient and K_c. If a temperature independent association rate coefficient is used, appropriate to this temperature ($k = 1.21 \times 10^{-11}$ cm^3 $molecule^{-1}$ s^{-1}) much better agreement is obtained (∼0.1% difference). At lower pressures, similar comparisons for k_3 showed differences of 10% and 6% for the T-dependent and T-independent forms of the association rate coefficient, respectively. The origin of these differences is not clear

(iii) k_4. Reactions R4 and R−4 do not make a substantial contribution to the reactivity of the system, because TS1 and TS2 present much lower energy dissociation routes for HSO_2 and for HOSO respectively, and the corresponding rate coefficients exceed those for (R4) and (R−4) by at least 3 orders of magnitude under conditions where these reactions are significant. The Bartis and Widom (or Klippenstein and Miller)[11,12] analysis does, however, provide a means of calculating k_4 and k_{-4}, which was not feasible in our earlier approach which relied on fitting species time profile.

Initially substantial differences were found between the rate coefficient ratio and K_4 reaching about 2 orders of magnitude at ∼30 atm and 1000 K. Further investigation suggested that these differences are related to detailed balance in the following way.

When a microcanonical ME is formulated, regardless of whether it is for a conservative system or not, the elements of the collision matrix are constrained to obey detailed balance. This endows the collision matrix with the useful property that it can be symmetrized by a similarity transformation (based on the equilibrium distribution). This has two benefits, it ensures that the eigenvalues are real and it allows the use of efficient symmetric matrix methods to calculate the eigenpairs. Equation E5 is isomorphic with the microcanonical ME from which it is derived. The equation is a ME in its own right and governs the evolution of the probability that a system will be located in a given well; these probabilities are related to the concentrations by a constant factor. Given this isomorphism the solution of eq E5 must be of the same form as that for the microcanonical ME. It is of interest to apply the standard procedure for symmetrizing a ME using a similarity transform based on the equilibrium distribution of the chemical system (in the absence of any sink terms). If this transform is denoted then

$$\frac{d\mathbf{g}}{dt} \mathbf{F}_c^{-1}\mathbf{Z}\Lambda'\mathbf{Z}^{-1}\mathbf{F}_c\mathbf{g} = \mathbf{W}\Lambda'\mathbf{W}^{-1}\mathbf{g} \qquad \text{(E13)}$$

Making this transform does not guarantee that the matrix $\mathbf{W}\Lambda'\mathbf{W}^{-1}$ is symmetric. However, since it is known that the eigenvalues of this matrix must be real (because they are the CSE from the microcanonical ME), then the matrix will be symmetric if the matrix $\mathbf{W}$ is orthogonal, or, equivalently, the rate coefficient matrix obeys detailed balance. Furthermore, if $\mathbf{W}$ is orthogonal it is straightforward to derive orthogonality relations similar to those given by Bartis and Widom.[12]

In analyzing the present system it was useful to employ these relations in order to assess how far the rate coefficient matrix deviated from detailed balance. Across a wide range of conditions, differences were minor, but for the conditions described above, there was a significant deviation from orthogonality, in particular the $\mathbf{W}$ eigenvector associated with λ_3 was significantly less than unit magnitude. Orthogonality can be imposed by using a Gram−Schmidt procedure, and when this was done for the H/SO_2 system, k_4 and k_{-4} became consistent with the equilibrium constant. This is, perhaps, not very surprising as imposing orthogonality is equivalent to imposing detailed balance. For the present system the impact of this imposition was minor because k_4 and k_{-4} only make a small contribution, the amended rate equations producing nearly identical concentrations. (One procedural benefit in imposing orthogonality is that the inversion of $\mathbf{W}$, and therefore $\mathbf{Z}$, requires only the taking of a transpose, making integration of the rate equations trivial.)

4.7. Bimodal Pressure Dependences in Rate Coefficients. The pressure dependences in the rate coefficients for reactions R1 and R2, shown in Figure 6, parts a and b, are as expected for association reactions; the reverse reactions behave similarly. k_3 shows the behavior expected for a reaction in which there is competition between reaction from the energized states produced from $H + SO_2$ and stabilization to form HOSO. The rate coefficient for reaction R6, on the other hand, shows an unusual bimodal form. The point of inflection occurs at ∼10 atm, increases only slowly with temperature, and is roughly coincident with the region in which k_3 starts to decrease. A possible explanation of this behavior is a significant change in the population distribution in the grains of the appropriate species. For example, at low pressures reaction from the highly energized states of HOSO are ascribed to direct reaction from $H + SO_2$, because there has been no, or little, collisional stabilization. In addition, the lower barrier for dissociation to $H + SO_2$ depletes these energized states.

5. Parametrization of Rate Coefficients

Temperature and pressure dependent rate coefficient expressions for the reactions given in Table 3 were obtained by fitting the Bartis and Widom generated rate coefficients to a Troe factorization model [28]

$$k(T,M) = \frac{k^{\infty}k^{0}[\mathrm{M}]}{k^{\infty} + k^{0}[\mathrm{M}]}F \qquad \text{(E14)}$$

where

$$\log F = \frac{\log F_c}{1 + \left(\frac{K}{N - 0.14K}\right)^2} \qquad \text{(E15)}$$

where $K = \log(k^{\circ}[\mathrm{M}]/k^{\infty}) + c$, $c = -0.4 - 0.67\log(F_c)$ and $N = 0.75 - 1.27\log(F_c)$

The temperature parametrization employed for F_C was

$$F_C = (1 - A)\exp(-T/T^{***}) + A\exp(-T/T^{*}) \qquad \text{(E16)}$$

Examples of fits are shown in Figure 6, parts a and b, and the Troe parameters are given in Table 3. Parameters are only given for the forward reactions, but equilibrium constants are also provided in Table 3 and can be used to calculate rate coefficients for the reverse reactions, subject to the limitations discussed in section 4.6. Some rate coefficients could not be fitted to eq E14. k_3 is given by[29]

$$k(T,M) = \frac{k^{\infty}k^{0}}{k^{\infty} + k^{0}[\mathrm{M}]}F \qquad \text{(E17)}$$

The bimodal behavior of k_6, k_4, and k_{-4} led to fitting difficulties. Because reactions R4 and R−4 make only a very minor contribution to the reaction, no attempt was made to fit k_4 and k_{-4}. Similarly, reaction R6 is unimportant at lower pressures below 10^3 atm. This restriction presents no practical problems, since reaction R−2 dominates the dissociation of HOSO at lower pressures, while reaction R3 dominates the formation of OH + SO from H + SO_2.

6. Comparison with Other Data

Parts a−c of Figure 8 show comparisons of the present rate data, at 1 atm, with rate coefficients from Goumri et al.[5] and from the analysis that we previously reported, based on a phenomenological treatment of the calculated concentrations of H, HSO_2 and HOSO. That treatment is superseded by the present analysis, because of the improvements that have been made in the approach and the modifications to the potential energy surface, based on experimental measurements of k_1. The large difference in k_6 at 1 atm arises from the previous use of an inappropriate Troe fit, which substantially overestimated k_6. The results from the present work, which are shown in Figure 8c, are derived directly from the Bartis and Widom analysis and not from the Troe fit, which is invalid in this pressure range. Note that $k_{-2} \gg k_6$ under these conditions.

As discussed in the Introduction, Glarborg[8] and Dagaut and co-workers[7] examined the role of H + SO_2 in studies of the effects of NO and SO_2 on the oxidation of CO/H_2 mixtures at temperatures in the range 800−1400 K and at 1 atm. Their mechanism included reaction 2 and utilized the rate coefficient of Goumri et al., which, at 1 atm, is close to that determined here. HOSO reacted with H to form H_2 + SO_2 and with O_2 to form HO_2 + SO_2, so that, in effect, SO_2 acted as a third body for H + H and H + O_2. The main impact of the present analysis on this mechanism is to increase the lifetime of HOSO, compared with rate constants based on the analysis of Hughes et al.,[10] through the reduction in k_6 (Figure 8c).

Hughes et al.[9] found that reaction 3 was the most important route for SO_2 destruction in a seeded, low-pressure methane + oxygen + argon laminar flame, operating at temperatures in the range 600−1800 K. They used the results derived from Blitz et al.[3] in their simulations, and the present analysis shows little change in the rate coefficient (Figure 8d). It is important to note that this result is closely linked to the strong negative dependence observed by Blitz et al.[3] for the rate coefficient for OH + SO; experiments at temperatures higher than those investigated in the latter study (<700 K) would be of value.

7. Summary and Conclusions

1. The H + SO_2/HSO_2/HOSO system has been studied using a combination of experiment and master equation analysis.

• The measurements were restricted to low temperatures (≤423 K), but allowed determination of k_1, the rate constant for HSO_2 formation. As a result, it was possible to refine the ab initio barrier to this reaction and the energy transfer parameter.

• The refined ab initio parameters were used in a master equation analysis that covered the temperature and pressure ranges 200−1700 K and 10^{-3}−10^6 atm, respectively. The ME is nonconservative, with the products OH + SO acting as a sink.

2. The three eigenvalues of smallest magnitude from the ME analysis correspond to the chemically significant eigenvalues of the system. Except at higher temperatures, they are well separated from the eigenvalues describing collisional relaxation.

3. Analysis of eigenpairs, based on developments by Bartis and Widom (BW) and by Klippenstein and Miller (KM), allowed canonical rate coefficients to be determined for each of the reaction steps in the chemical system. The initial analysis using the BW approach led to some discrepancies between ratios of rate coefficients and equilibrium constants; no such problem was encountered with the KM approach. This problem was removed if orthogonality was imposed on the matrix governing the evolution of the chemical system.

4. The chemically significant eigenvalues were well separated from one another, because of the increasing height of the activation barriers linking H + SO_2 to HSO_2, to HOSO, and to OH + SO. To a good approximation, each eigenvalue is associated with passage over a single activation barrier. This conclusion is based on an examination of the relationship between the eigenvalues and combinations of rate coefficients, based on an approximate analysis of the evolution of the chemical system and limiting low and high temperatures.

5. The rate coefficients for the main reactions in the system were parametrized using the Troe formalism (R1, R−1, R2, R−2) and using a modified expression for k_3. From a combustion perspective, the key reactions are those governing the production and removal of HOSO (R2 and R−2 and, at very high pressures, R6). The main route to OH+ SO from H + SO_2 occurs via reaction R3, which proceeds via energized states of HOSO, but does not involve stabilization into the HOSO well for pressures ≤10^3 atm. The microcanonical rate constants used for dissociation to form OH + SO from HOSO* were based on the experimental measurements of k(OH + SO) by Blitz et al., which were limited to temperatures below ∼700 K. The main uncertainty in the calculation of k_3 is the temperature dependence of k(OH + SO); further experiments, at higher temperatures, are needed.

Acknowledgment. The authors are grateful to EPSRC for funding and to Peter Glarborg and Paul Marshall for helpful discussions.

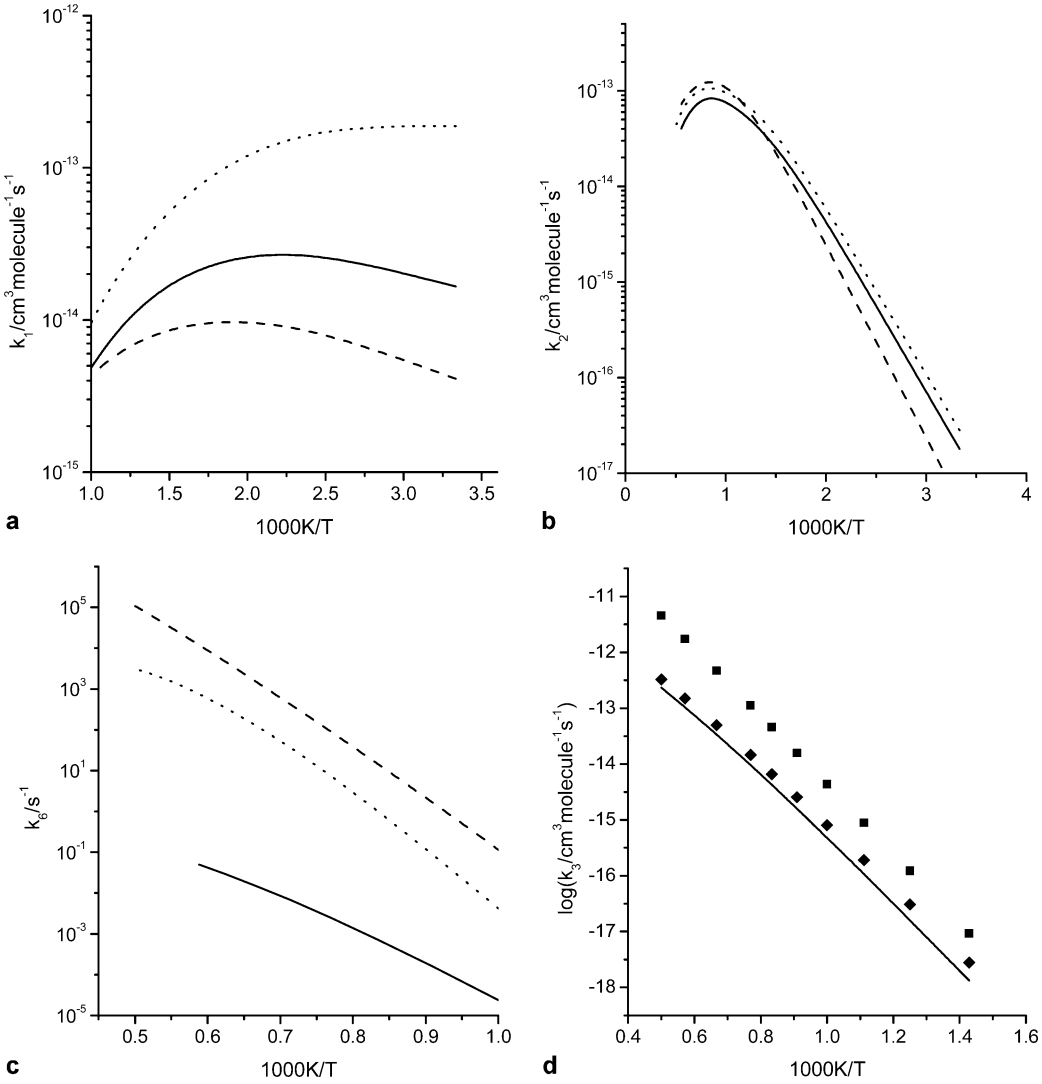

Figure 8. Comparison of rate coefficients at 1 atm as a function of temperature: (a) k_1; (b) k_2; (c) k_6; (d) k_3. Key: (−) this work; (···) Hughes et al.[10] ; (- -) Goumri et al.;[5] (■) Jourdain et al.;[2] (◆) Blitz et al. The data from the current work are from Troe or modified Troe fits (eqs E14 and E17) except for k_6, where the data obtained directly from the Bartis and Widom analysis is shown, because a Troe fit was not feasible.

Appendix A

Method Used To Extract Canonical Rate Coefficients from Master Equation Calculations. In this appendix, an outline will be given of how canonical rate coefficient data can be extracted from the master equation. The most recent approach to this problem is that of Klippenstein and Miller.[11] The outline given here, and used in the analysis of the ME data above, differs slightly from that of Bartis and Widom [12] in that the coefficients of the eigenvector expansion, which depend on the initial distribution, do not appear in the expressions for the rate coefficients which are therefore independent of the initial concentrations. The basis of the approach is to begin with the ME describing the microscopic evolution of the system and derive from it a reduced set of equations of motion that described the evolution of the macroscopic concentrations. Starting with the ME for an n component system (i.e., eq E3 of section 4.1):

$$\frac{d\mathbf{p}}{dt} = \mathbf{M}\mathbf{p} \tag{A1}$$

the concentration of, e.g., species A is given

$$[A](t) = \sum_{i\in A} p_i(t) \tag{A2}$$

Differentiating this expression with respect to t gives

$$\frac{d[A]}{dt} = \sum_{i\in A}\frac{dp_i}{dt} = \sum_{i\in A}(\mathbf{M}\mathbf{p})_i = \sum_{i\in A}(\mathbf{U}\Lambda\mathbf{U}^{-1}\mathbf{p})_i \tag{A3}$$

where Λ is a diagonal matrix of the eigenvalues of **M** and **U** is a matrix of the associated eigenvectors. Expanding the right-hand side of eq A3 in terms of the matrix components and invoking the diagonal property of Λ gives

$$\frac{d[A]}{dt} = \sum_{i\in A}\sum_{l}\sum_{j} U_{il}\Lambda_l U_{lj}^{-1} p_j \tag{A4}$$

Defining Z_{Al} as

$$Z_{Al} = \sum_{i\in A} U_{il} \tag{A5}$$

and substituting into eq A4 give

$$\frac{d[A]}{dt} = \sum_{l}\sum_{j} Z_{Al}\Lambda_l U_{lj}^{-1} p_j = \sum_{j} Z_{Al}\Lambda_l c_l \tag{A6}$$

From eq A6, it follows that that the population vector **p** can be

written in terms of the vector **c** as

$$\mathbf{p} = \mathbf{Uc} \tag{A7}$$

Applying eqs A2 and A5 yields

$$[\mathrm{A}](t) = \sum_l Z_{\mathrm{A}l} c_l \tag{A8}$$

or defining a vector whose elements are the concentrations of each species,

$$\mathbf{r} = \mathbf{Zc} \tag{A9}$$

from which the vector **c** could be obtained if the matrix **Z** is invertible. The matrix **Z** is constructed by adding elements of all the eigenvectors over ranges that correspond to each of the species involved in the reaction and, in general, is not a square matrix. While it is possible to define an inverse for **Z** in some circumstances, it cannot be done for the present situation.

However, the region of interest is after the short transient period, and in this region, the evolution of the system is, for a system of *n* interconnecting wells, governed by *n* eigenvalues. Bartis and Widom used this fact to truncate the expansion in eq A4 to terms in chemically significant eigenvalues. Under these conditions the matrix **Z** becomes square and can be inverted to yield the vector **c**. Substitution of the result into eq A6 and recasting in terms of the vector **r** gives a set of equations of motion for the macroscopic concentrations:

$$\frac{\mathrm{d}\mathbf{r}}{\mathrm{d}t} = \mathbf{Z}\Lambda'\mathbf{Z}^{-1}\mathbf{r} = \mathbf{K}_\mathrm{r}\mathbf{r} \tag{A10}$$

where Λ' is a diagonal matrix of dimension *n* with the *n* largest eigenvalues on its leading diagonal. Since the elements of **Z** depend only on the elements of the eigenvectors it follows that the matrix $\mathbf{K}_\mathrm{r}$ is independent of time and the initial distribution of the system. Consequently, the equations of motion are linear in the concentrations, and the elements of matrix $\mathbf{K}_\mathrm{r}$ are the rate coefficients connecting the wells and for reactive loss.

Bartis and Widom investigated the properties of the elements of $\mathbf{K}_\mathrm{r}$, and using an approximate orthogonality condition derived from a quantum mechanical analogue, they showed that, for a conservative system, detailed balance was obeyed at the macroscopic level.

It is straightforward to integrate (phenomenological) equation (A10) and this was done for the H + SO_2 system and the concentrations compared with those generated from the ME. The phenomenological concentrations compared well over a wide range of conditions, with deviations occurring only at short times (as expected) or at high temperatures where the number of significant eigenvalues increases and so the phenomenological rate equations no longer apply.

References and Notes

(1) Fair, R. W.; Thrush, B. A. *Trans. Faraday Soc.* **1969**, *65*, 1550.
(2) Jourdain, J. L.; Le Bras, G.; Combourieu, J. *Int. J. Chem. Kinet.* **1979**, *11*, 569.
(3) Blitz, M. A.; McKee, K. W.; Pilling, M. J. *Proc. Combust. Inst.* **2000**, *28*, 2491.
(4) Frank, A. J.; Sadilek, M.; Ferrier, J. G.; Turecek, F. *J. Am. Chem. Soc.* **1997**, *119*, 12343.
(5) Goumri, A.; Rocha, J.-D. R.; Laakso, D.; Smith, C. E.; Marshall, P. *J. Phys. Chem. A* **1999**, *103*, 11328.
(6) Alzueta, M. U.; Bilbao, R.; Glarborg, P. *Combust. Flame* **2001**, *127*, 2234.
(7) Dagaut, P.; Lecomte, F.; Mieritz, J.; Glarborg, P. *Int. J. Chem. Kinet.* **2003**, *35*, 564.
(8) Glarborg, P.; Kubel, D.; DamJohansen, K.; Chiang, H. M.; Bozzelli, J. W. *Int. J. Chem. Kinet.* **1996**, *28*, 773.
(9) Hughes, K. J.; Tomlin, A. S.; Dupont, V. A.; Pourkashanian, M. *Faraday Discuss.* **2001**, *119*, 337.
(10) Hughes, K. J.; Blitz, M. A.; Pilling, M. J.; Robertson, S. H. *Proc. Combust. Inst.* **2002**, *29*, 2431.
(11) Klippenstein, S. J.; Miller, J. A. *J. Phys. Chem. A* **2002**, *106*, 9267.
(12) Bartis, J. T.; Widom, B. *J. Chem. Phys.* **1974**, *60*, 3474.
(13) Blitz, M. A.; Johnson, D. G.; Pesa, M.; Pilling, M. J.; Robertson, S. H.; Seakins, P. W. *J. Chem. Soc., Faraday Trans.* **1997**, *93*, 1473.
(14) Blitz, M. A.; Hughes, K. J.; Pilling, M. J. *J. Phys. Chem. A* **2003**, *107*, 1971.
(15) Wine, P. H.; Nicovich, J. M.; Hynes, A. J.; Wells, J. R. *J. Phys. Chem.* **1986**, *90*, 4033.
(16) Wallenstein, R. *Opt. Commun.* **1980**, *33*, 119.
(17) Barone, S. B.; Turnipseed, A. A.; Gierczak, T.; Ravishankara, A. R. *J. Phys. Chem.* **1994**, *98*, 11969.
(18) Okabe, H. *Photochemistry of Small Molecules*; Wiley: New York, 1978.
(19) Rao, T. N.; Calvert, J. G. *J. Phys. Chem.* **1970**, *74*, 681.
(20) Cox, R. A. *J. Phys. Chem.* **1972**, *76*, 814.
(21) Partymiller, K.; Heicklen, J. *J. Photochem.* **1977**, *7*, 221.
(22) Pilling, M. J.; Robertson, S. H. *Annu. Rev. Phys. Chem.* **2003**, *54*, 245.
(23) Blitz, M. A.; Beasley, M. S.; Pilling, M. J.; Robertson, S. H. *Phys. Chem. Chem. Phys.* **2000**, *2*, 805.
(24) Holbrook, K. A.; Pilling, M. J.; Robertson, S. H. *Unimolecular Reactions*, 2nd ed.; Wiley: Chichester, New York, 1996.
(25) Davies, J. W.; Green, N. J. B.; Pilling, M. J. *Chem. Phys. Lett.* **1986**, *126*, 373.
(26) Anderson, E.; Bai, Z.; Bischof, C.; Demmel, J.; Dongarra, J.; Du Croz, J.; A.; G.; Hammarling, S.; McKenney, A.; Ostrouchov, S.; Sorensen, D. *LAPACK user's guide*; SIAM: Philadelphia, PA, 1992.
(27) DeSain, J. D.; Klippenstein, S. J.; Miller, J. A.; Taatjes, C. A. *J. Phys. Chem. A* **2004**, *108*, 7127.
(28) Troe, J. *Ber. Bunsen-Ges. Phys. Chem.* **1974**, *78*, 478.
(29) Pereira, R. D. A.; Baulch, D. L.; Pilling, M. J.; Robertson, S. H.; Zeng, G. *J. Phys. Chem. A* **1997**, *101*, 9681.